Effect of Sb on the Microstructure and Mechanical Properties of AZ91 Magnesium Alloy

QUDONG WANG, WENZHOU CHEN, WENJIANG DING, YANPING ZHU, and M. MABUCHI

Effects of Sb addition on the microstructure, mechanical properties, and fracture behaviors of AZ91 magnesium alloy, as well as the sensitivity to section thickness of the structure and mechanical properties, have been studied. The results show that when Sb is added into the AZ91 alloy, the grain is refined, the $Mg_{17}Al_{12}$ phase is refined and granulated, and a new Mg_3Sb_2 phase is formed and becomes coarse needle-shaped as Sb content increases. The room-temperature tensile strength, elongation, and impact toughness increase first, and then decrease with increasing Sb content. The study on sensitivity to section thickness shows that, when composition is constant, the room-temperature tensile strength and elongation increase with the reduction of section thickness; when section thickness is constant, the room-temperature tensile strength and elongation increase first, and then decrease with increasing Sb content. Additionally, the Sb addition improves the tensile strength of the AZ91 alloy at 100 °C and 150 °C. The room-temperature tensile and impact fractographs of the AZ91 alloy show intergranular fracture. With increasing Sb content, the tearing deformation zones on the both fractographs enlarge at first, and then diminish, which is consistent with the change of tensile strength, elongation, and impact toughness increasing first, and then reducing with increasing Sb content.

I. INTRODUCTION

THE magnesium alloy, as the lightest structural metal, has been widely used in automobile, electronics and aerospace industries[1–4] due to its desirable combination of properties, including low density, high specific strength and specific stiffness, superb damping and electromagnetic shielding capacities, excellent machinability, and good castability.[5] However, only a small amount of R&D has been carried out on it as compared with the aluminum alloy, and its applications are also limited.[6] Principal reasons for this are its relatively poor mechanical properties at room and elevated temperature.[7]

Although some Mg alloys have obtained, good creep resistance at elevated temperature by alloying with some costly elements such as Zr, Ag, Y, Th, and RE,[8] the usage of these expensive alloys are restrained to high-performance engines such as in Formula 1 race cars, air plane, and missiles.[9,10] This situation demands for intensive research to be conducted on the effects of alloying elements on the microstructure and properties of the Mg alloy.[11] Antimony is a surface-active element extensively used as a modifier in Al-Si alloys.[12] It was found that the addition of Sb into the Mg alloy results in grain refinement[13] and formation of compounds on grain boundaries,[14] which can improve room and elevated temperature strength,[15] creep properties,[16] and even fluidity.[11] Thus, Sb is considered as an important element to replace the RE partially or to take the place of Ag for future high strength Mg alloy development and the existing alloy modification.[11] However, it is also commonly held that Sb can impair plasticity and ductility.[17] Pekguleryuz suggested that further investigation should be performed on the effects of Sb on the microstructure and mechanical properties of Mg alloys, especially for Mg alloys containing the Zn and Al, given the low elongation of Mg-Sb binary alloy.[11] In this study, the effects of Sb on the microstructure and mechanical properties of AZ91, the most widely used Mg alloy to date, have been investigated.

II. EXPERIMENTAL

The present alloys were prepared using AZ91 alloy ingots and metal Sb. Table I shows the chemical compositions of the alloys. The melting was carried out in a 20 kg resistance crucible furnace. Antimony was added at 600 °C to 650 °C. The melt of the magnesium alloy was refined at 720 °C to 730 °C and then held for 20 minutes before pouring. The cover flux was added before charging and during melting to prevent ignition.

The ambient temperature tensile specimens with a diameter of 16 mm were cast in a metal mold. The same specimens were machined to make double thread tensile specimens with a diameter of 5 mm, which were used in the elevated temperature tensile test, as before.[18] The plate tensile specimens with thickness of 11, 9, 6, 4.5, 3 and 2 mm were cast in a metal mold to test the sensitivity to section thickness of microstructure and tensile properties. The impact specimens without notch were cast to 10 × 10 × 70 mm in a metal mold and used to test the impact toughness of the alloys at ambient temperature. All tensile tests were carried out on a SHIMADZU AG-100KNA materials testing machine at a tensile speed of 1 mm/min. The impact toughness was measured using an XJJ-50J impact-testing machine.

The metallographic observations were performed on the cross sections of the plate tensile specimens and the ambient temperature tensile specimens (the gage length portion). The phases in the specimens were analyzed by means of a D/MAX-IIIA X-ray diffractometer. The tensile and impact

QUDONG WANG and YANPING ZHU, Associate Professors, WENZHOU CHEN, Graduate Student, and WENJIANG DING, Professor, are with the State Key Laboratory of Metal Matrix Composites, Shanghai Jiaotong University, Shanghai 200030, People's Republic of China. M. MABUCHI, Senior Researcher, is with National Industrial Research Institute of Nagoya, 1-1 Hirate-cho, Kita-ku, Nagoya 462-8510, Japan.

Manuscript submitted December 29, 1999.

Table I. Chemical Compositions of Used Alloy (Weight Percent)

	Al	Zn	Mn	Sb	Be	Fe	Cu	Si	Ni
AZ91	8.12	0.923	0.142	—	0.00067	0.0148	<0.004	0.0607	0.0042
AZ91 + 0.5Sb	7.27	0.849	0.162	0.48	0.00050	0.0118	<0.004	0.0502	0.0029
AZ91 + 1.0Sb	7.04	0.891	0.160	0.94	0.00045	0.0138	<0.004	0.0485	0.0066
AZ91 + 2.0Sb	6.85	0.906	0.168	2.10	0.00050	0.0250	<0.004	0.0527	0.0211

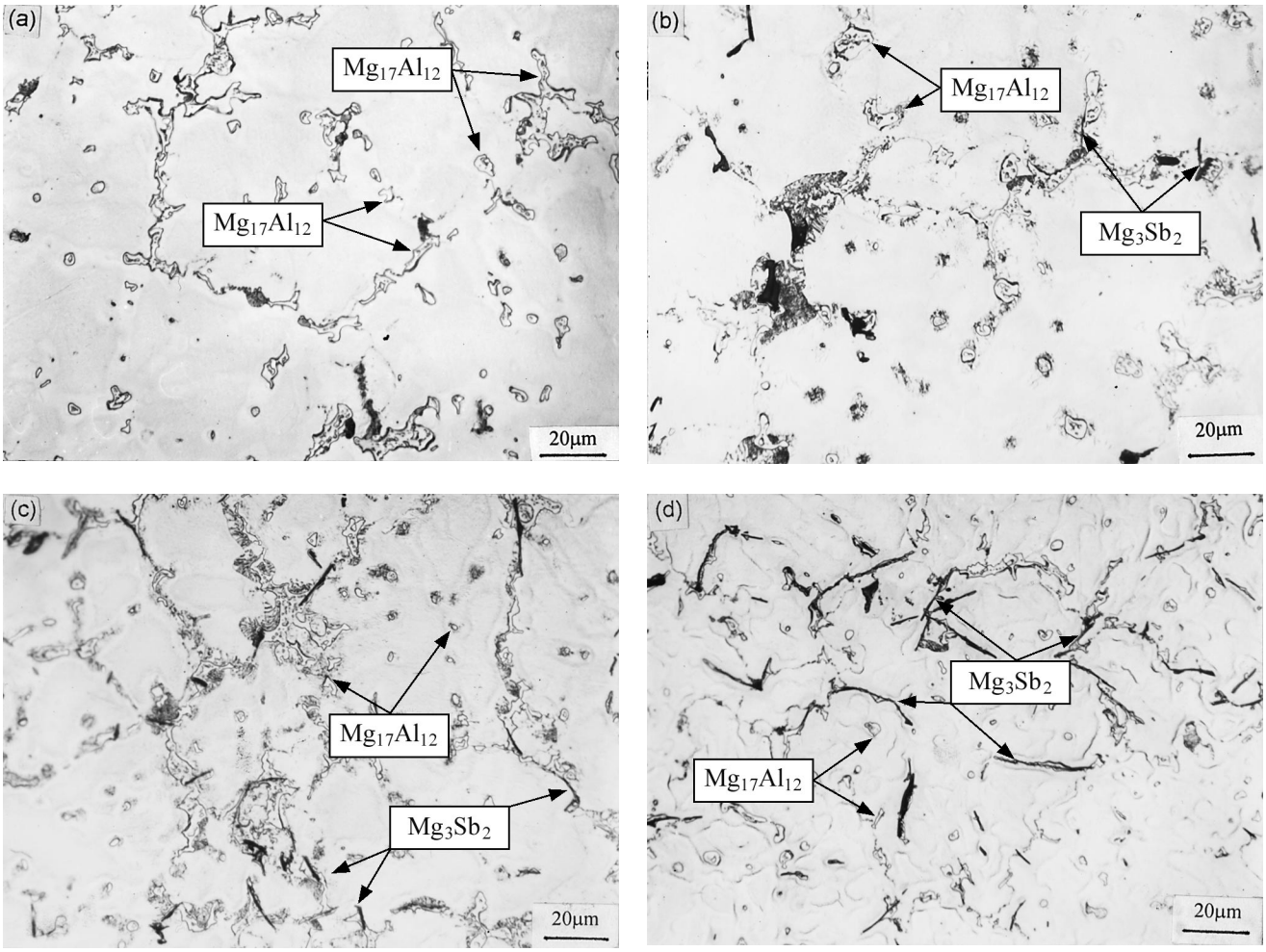

Fig. 1—Effects of Sb on the microstructure of AZ91 magnesium alloy (sample o.d. 16 mm): (*a*) AZ91, (*b*) AZ91 + 0.5Sb, (*c*) AZ91 + 1Sb, and (*d*) AZ91 + 2Sb.

fractographs were observed by a PHILIPS* SEM515 and S520 scanning electron microscope (SEM). The compositions of the phases were analyzed quantitatively using an energy-dispersive spectroscope (EDS) attached to the S520 SEM.

*PHILIPS is a trademark of Philips Electronic Instruments Corp., Mahwah, NJ.

III. RESULTS AND DISCUSSION

A. *The Effects of Sb Addition on the Microstructure*

Figure 1 shows that the effects of Sb addition on the microstructure of the tensile specimens for 16-mm diameter. When 0.5 wt pct Sb is added, the grain refinement occurs, the amount of granular $Mg_{17}Al_{12}$ phase increases, while the amount of irregular-shaped and strip $Mg_{17}Al_{12}$ phase on grain boundaries decreases, and a small amount of new black strip phase (Mg_3Sb_2, identified by EDS) is formed. Besides, the amount of α-Mg-$Mg_{17}Al_{12}$ eutectic on grain boundaries or secondary $Mg_{17}Al_{12}$ phase in Mg matrix also increases. When 1 wt pct Sb is added, the preceding effects become more obvious. When the Sb content increases to 2 wt pct, the grain size has no significant change, the amount and size of new Mg_3Sb_2 phase increases considerably, and the amount of α-Mg-$Mg_{17}Al_{12}$ eutectic or the secondary $Mg_{17}Al_{12}$ phase decreases considerably.

As was shown previously, a new Mg_3Sb_2 phase is formed with Sb addition, which is verified by both the results of EDS and X-ray analysis of AZ91-2.0Sb (Figure 2).

It can be observed that Sb addition into AZ91 does not appreciably change the quantity of the $Mg_{17}Al_{12}$ phase. This

result is due to the following reason: (1) the solubility of Sb in magnesium is very low,[19] (2) no Al-Sb compounds are formed after Sb addition, and (3) Al still forms $Mg_{17}Al_{12}$ with Mg after Sb addition.

Figure 3 shows the effects of Sb on the microstructure of the plate tensile specimen with the thickness of 2 mm. Compared with Figure 1, the effects of Sb addition are similar except that the grain, compounds, and eutectic are much finer in this case.

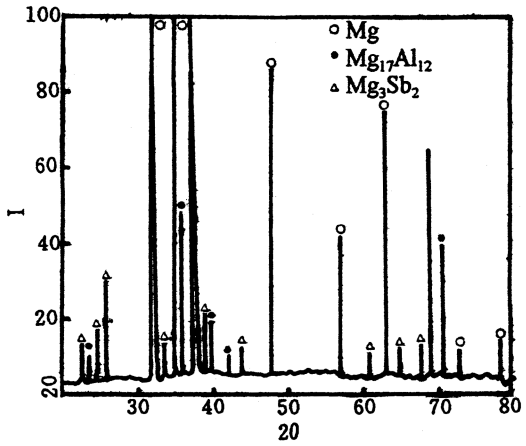

Fig. 2—Result of X-ray diffraction analysis on AZ91 + 2Sb magnesium alloy.

Figure 4 shows the effects of the section thickness on the microstructure of AZ91 + 0.5Sb. With the reduction of thickness, the sizes of grain and other phases decreases due to the increasing cooling rate, and the amount of secondary $Mg_{17}Al_{12}$ increases due to the reduction of diffusion distance resulting from the grain refinement.

B. *The Effects of Sb Addition on the Mechanical Properties*

Figure 5 shows the effects of Sb addition on the room-temperature mechanical properties of AZ91. The tensile strength (σ_b) and elongation (δ) increase at first with increasing Sb content, and then decrease when the Sb content exceeds 1 wt pct, reaching maximum when Sb content is 0.5 wt pct.

The preceding effects can be explained as follows. When Sb content is less than 1 wt pct, the grain refinement effect and the beneficially refined and granulated morphology of the compounds $Mg_{17}Al_{12}$ cause the increase of the tensile

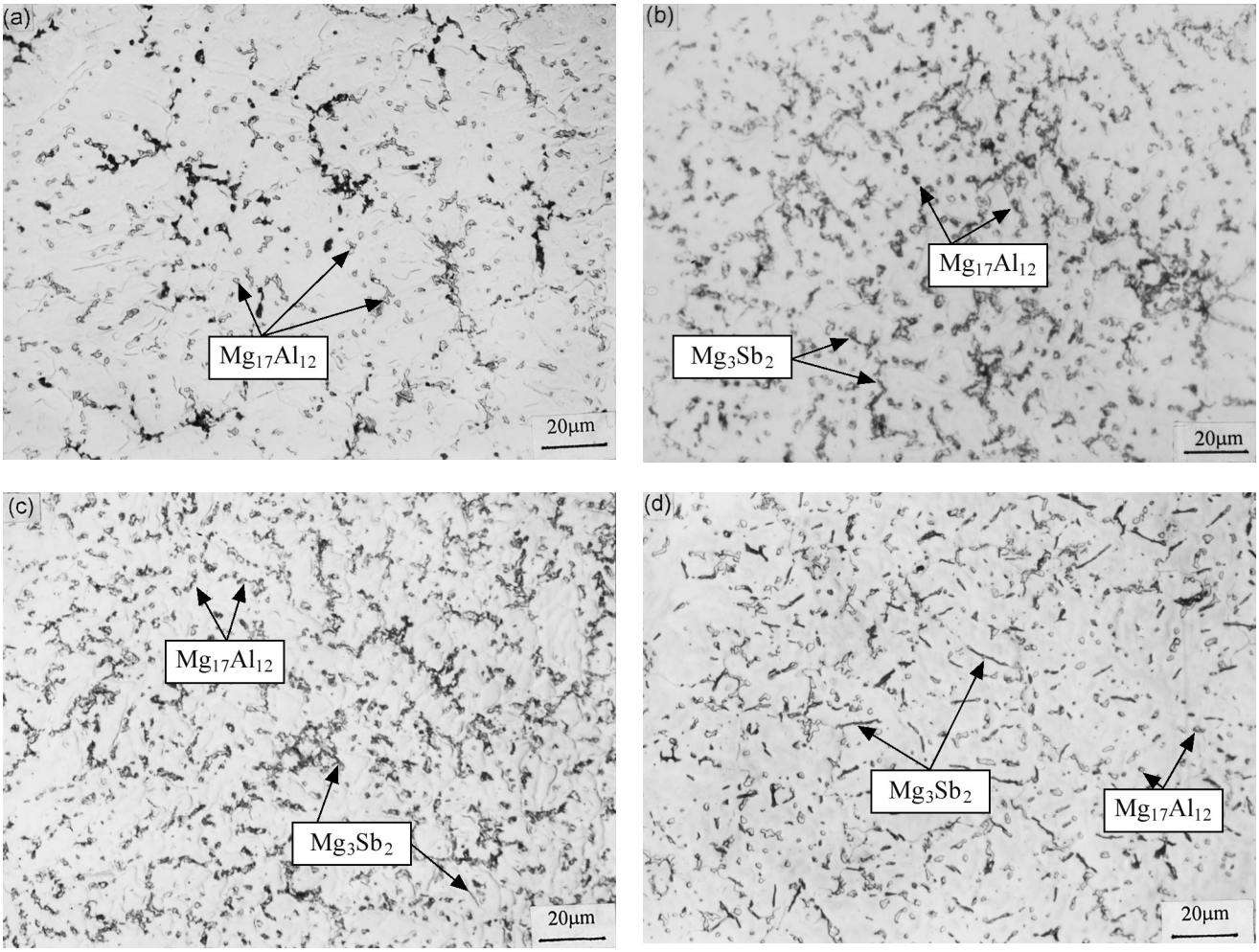

Fig. 3—Effects of Sb on the microstructure of AZ91 magnesium alloy (sample thickness 2 mm): (*a*) AZ91, (*b*) AZ91 + 0.5Sb, (*c*) AZ91 + 1Sb, and (*d*) AZ91 + 2Sb.

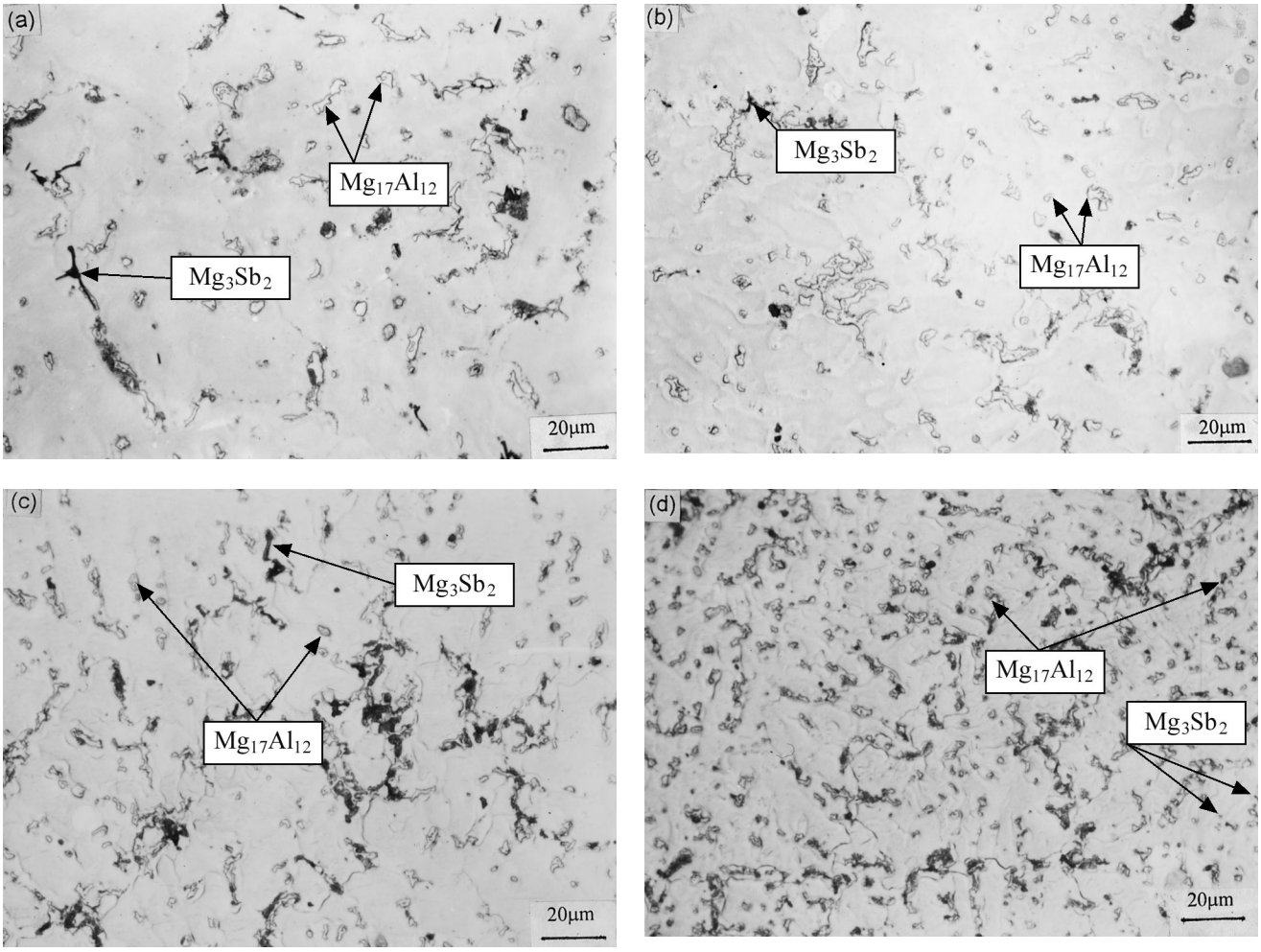

Fig. 4—Section sensitivity of microstructure of AZ91 + 0.5Sb magnesium alloy: (*a*) 11 mm, (*b*) 9 mm, (*c*) 6 mm, and (*d*) 4.5 mm.

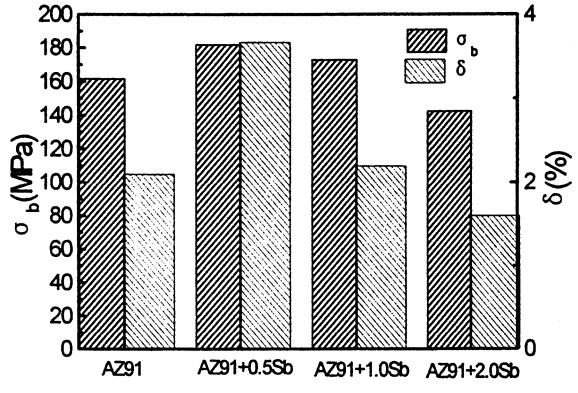

Fig. 5—Effects of Sb on the ambient mechanical properties of AZ91 magnesium alloy.

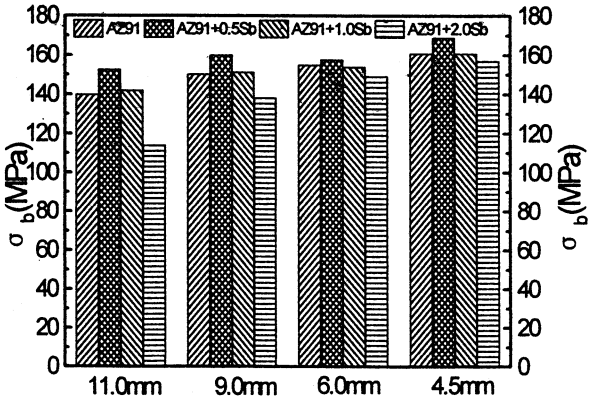

Fig. 6—Section sensitivity of tensile strength of AZ91 + Sb magnesium alloy (tensile strength (σ_b) vs section thickness).

strength and elongation. When Sb content is above 1 wt pct, the amount of needle-shaped Mg_3Sb_2 phase increases markedly, which dissevers matrix and causes the drop of the tensile strength and elongation. When the Sb content arrives at 2 wt pct, the tensile strength and elongation is even lower than AZ91 due to the presence of a large amount of needle-shaped Mg_3Sb_2 phase.

Figures 6 through 9 shows the sensitivity of the mechanical properties to the section thickness of Sb containing Mg alloy. Figures 6 and 7 show, as a whole, that the tensile strength increases with the reduction of section thickness when composition is constant, whereas the tensile strength increases, and then decreases with increasing Sb content, when the section thickness is constant. The tensile strength

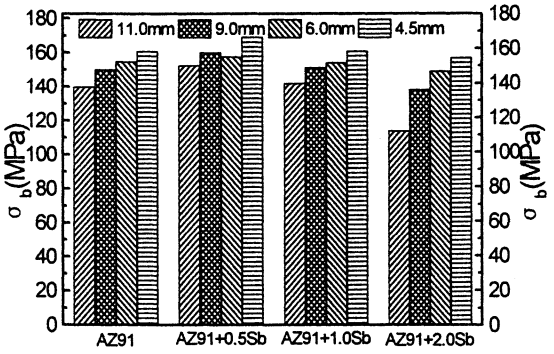

Fig. 7—Section sensitivity of tensile strength of AZ91 + Sb magnesium alloy (tensile strength (σ_b) vs alloy composition).

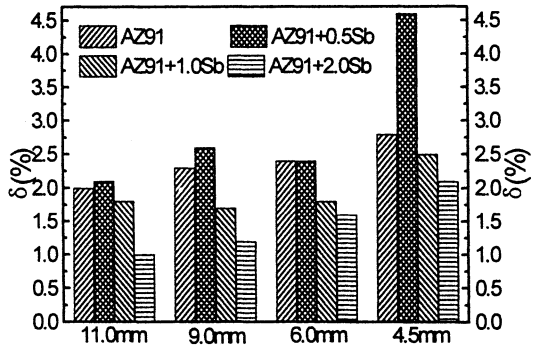

Fig. 8—Section sensitivity of elongation of AZ91 + Sb magnesium alloy (elongation (δ) vs section thickness).

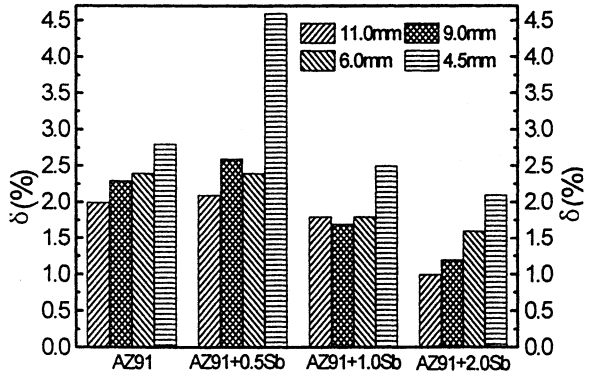

Fig. 9—Section sensitivity of elongation of AZ91 + Sb magnesium alloy (elongation (δ) *vs* alloy composition).

is highest for the all section thicknesses when the Sb content is 0.5 wt pct. Figures 8 and 9 show that similar effects can also be observed for elongation. The elongation is highest for all section thicknesses when the Sb content is 0.5 wt pct.

Figures 10 and 11 show the effects of Sb addition on the tensile properties of AZ91 at elevated temperature (100 °C and 150 °C). Figure 10 shows that the tensile strength and elongation of the Mg alloy at 100 °C increase at first and then decrease with increasing Sb content, reaching their maximum when Sb content is 1 and 0.5 wt pct, respectively. The tensile strength of all of the Mg alloys studied is higher than that of the AZ91 Mg alloy at 100 °C; the elongation of Sb containing Mg alloys (Sb $\leq$ 1 wt pct) is higher than

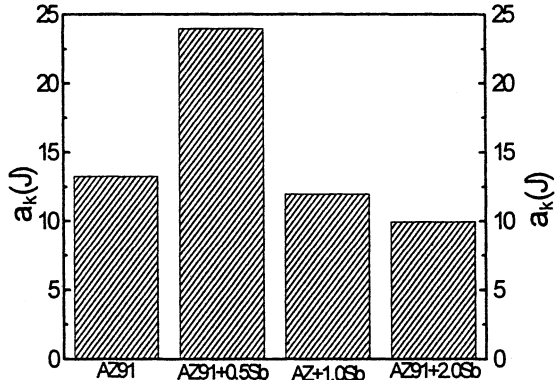

Fig. 10—Effects of Sb on the tensile strength (σ_b) and elongation (δ) of AZ91 magnesium alloy at 100 °C.

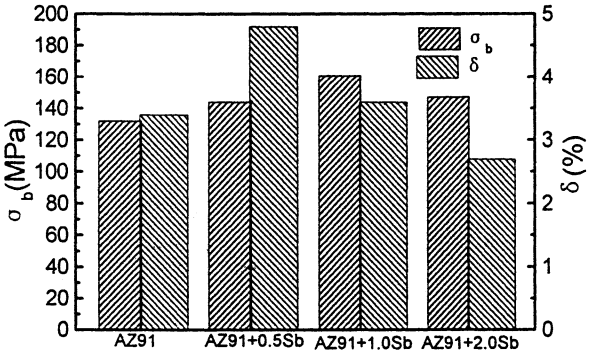

Fig. 11—Effects of Sb on the tensile strength (σ_b) and elongation (δ) of AZ91 magnesium alloy at 150 °C.

that of AZ91 Mg alloy at 100 °C. Figure 11 shows that the tensile strength of the Mg alloy at 150 °C also increases at first and then decreases with increasing Sb content, reaching maximum when Sb content is 1 wt pct. The tensile strength of all of the studied Sb containing Mg alloys is higher than that of AZ91 Mg alloy at 150 °C. However, the elongation of the Mg alloy at 150 °C decreases with increasing Sb content throughout the tested Sb content range.

In AZ91 alloy, the main strengthening phase is $Mg_{17}Al_{12}$, which has a low melting point (437 °C), and poor thermal stability. The $Mg_{17}Al_{12}$ phase can readily coarsen and soften at the temperatures exceeding 120 °C to 130 °C. [18] In addition, $Mg_{17}Al_{12}$ has a cubic crystal structure incoherent with the hcp magnesium matrix, which leads to the fragility of the $Mg/Mg_{17}Al_{12}$ interface. All of the preceding data lead to the poor elevated temperature tensile properties of AZ91 alloy (Figures 10 and 11).

The addition of Sb to AZ91 formed Mg_3Sb_2 precipitation in the alloy. The Mg_3Sb_2 has a much higher melting point (1228 °C), [19] which, along with the low diffusion speed of Sb in magnesium at elevated temperatures, makes Mg_3Sb_2 have a high thermal stability. So sliding of grain boundaries and growth of cracks were effectively prevented at elevated temperatures, elevated temperature tensile properties were improved and an obvious elevated temperature strengthening effect was obtained. However, a large amount of coarse strip Mg_3Sb_2 phase formed when excessive Sb is added cuts apart the alloy matrix, which results in a decrease of the strength

and especially a decrease of the elongation (Figures 10 and 11).

Figure 12 shows the effect of Sb addition on the impact toughness of AZ91. Impact toughness increases, and then decreases with increasing Sb content, reaching a maximum when Sb content is 0.5 wt pct. The improvement of impact toughness is attributable to grain refinement, refinement, and granulation of $Mg_{17}Al_{12}$ phase after a small amount of the Sb is added, while the presence of the needle-shaped compound Mg_3Sb_2 with excessive Sb causes the drop of impact toughness.

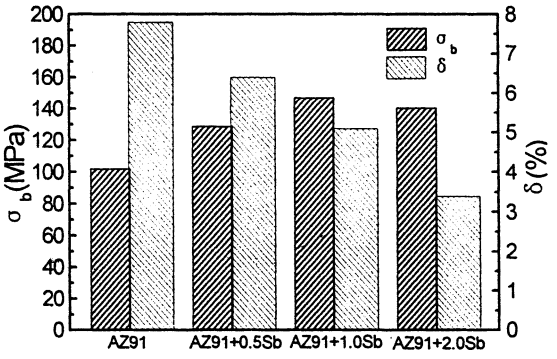

Fig. 12—Effects of Sb on the impact toughness of AZ91 magnesium alloy.

C. *The Effects of Sb Addition on the Fracture Mode*

Figure 13 is the tensile fractographs of AZ91 + *x*Sb showing an intergranular fracture feature. Figure 13(a) shows that plastic deformation is difficult to cause in AZ91. The fractographs exhibit intergranular fracture features with some secondary cracks (see arrowheads at A) on them. In addition, the dimpled quasi-cleavage fracture is also observed in some parts (Figure 13(a), at B in the middle); there are some small cleavage steps in the quasi-cleavage dimples, which are connected by the tearing ridges of different size. With Sb addition, the deformation zone on the fractograph of AZ91 + 0.5Sb enlarges considerably, as shown at C in Figure 13(b), which demonstrates its high tensile strength and elongation. Figure 13(c) shows that the fractograph of AZ91 + 1Sb possesses a smaller deformation zone (at C in Figure 13(c)) and correspondingly lower tensile strength and elongation than AZ91 + 0.5Sb; Figure 13(d) shows that the fractograph of AZ91 + 2Sb possesses the smallest deformation zone, exhibiting an entire intergranular fracture feature, and also the lowest tensile strength and elongation.

Figure 14 gives the impact fractographs of AZ91 + *x*Sb showing the intergranular fracture. Figure 14(a) shows that the impact fractograph of AZ91 has some cleavage steps (at D in Figures 14(a) and (c)) and more deformation tearing ridges (at C in Figure 14) than its tensile fractographs, also exhibiting intergranular fracture features. Figure 14(b)

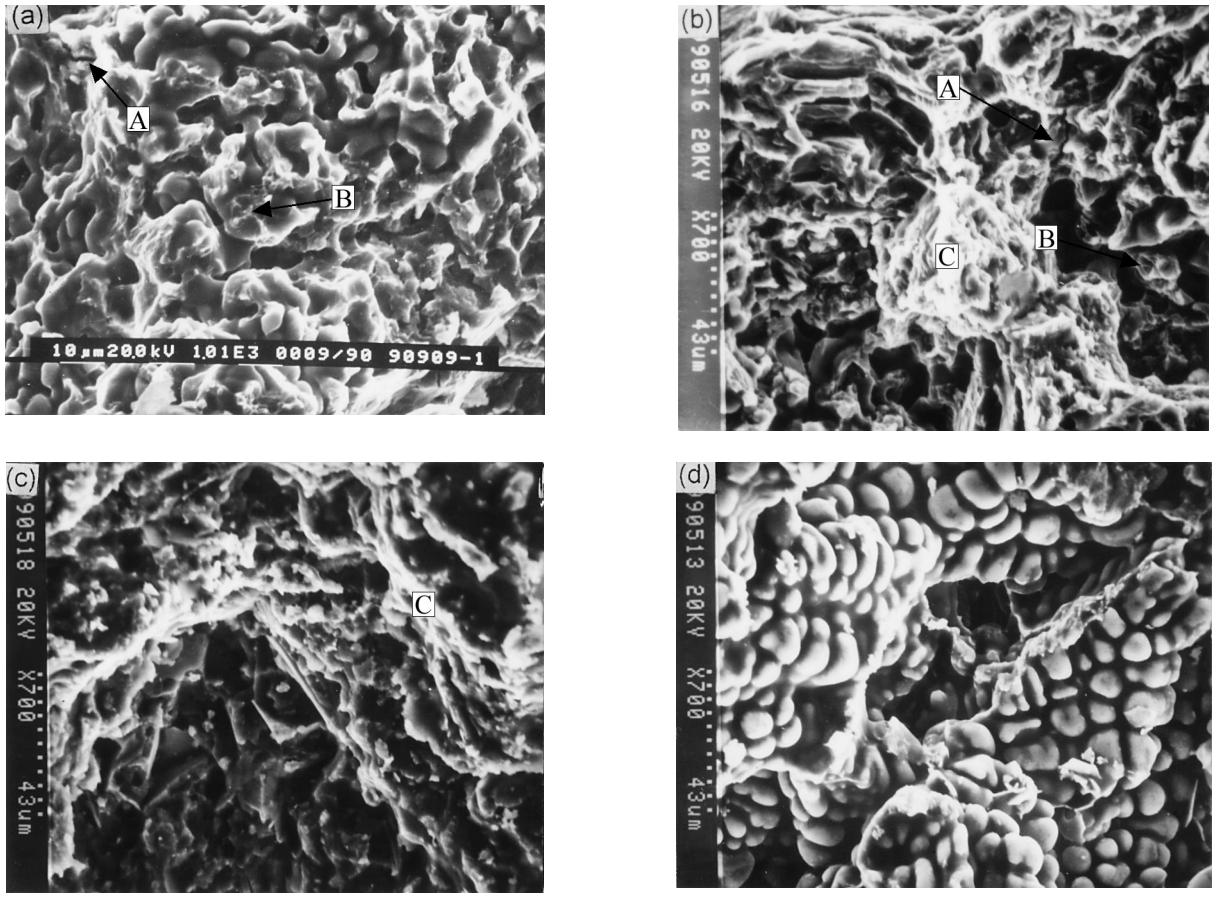

Fig. 13—Effects of Sb on the tensile fractographs of AZ91 magnesium alloy: (*a*) AZ91, (*b*) AZ91 + 0.5Sb, (*c*) AZ91 + 1Sb, and (*d*) AZ91 + 2Sb. A: secondary crack, B: quasi-cleavage dimple, and C: deformation zone.

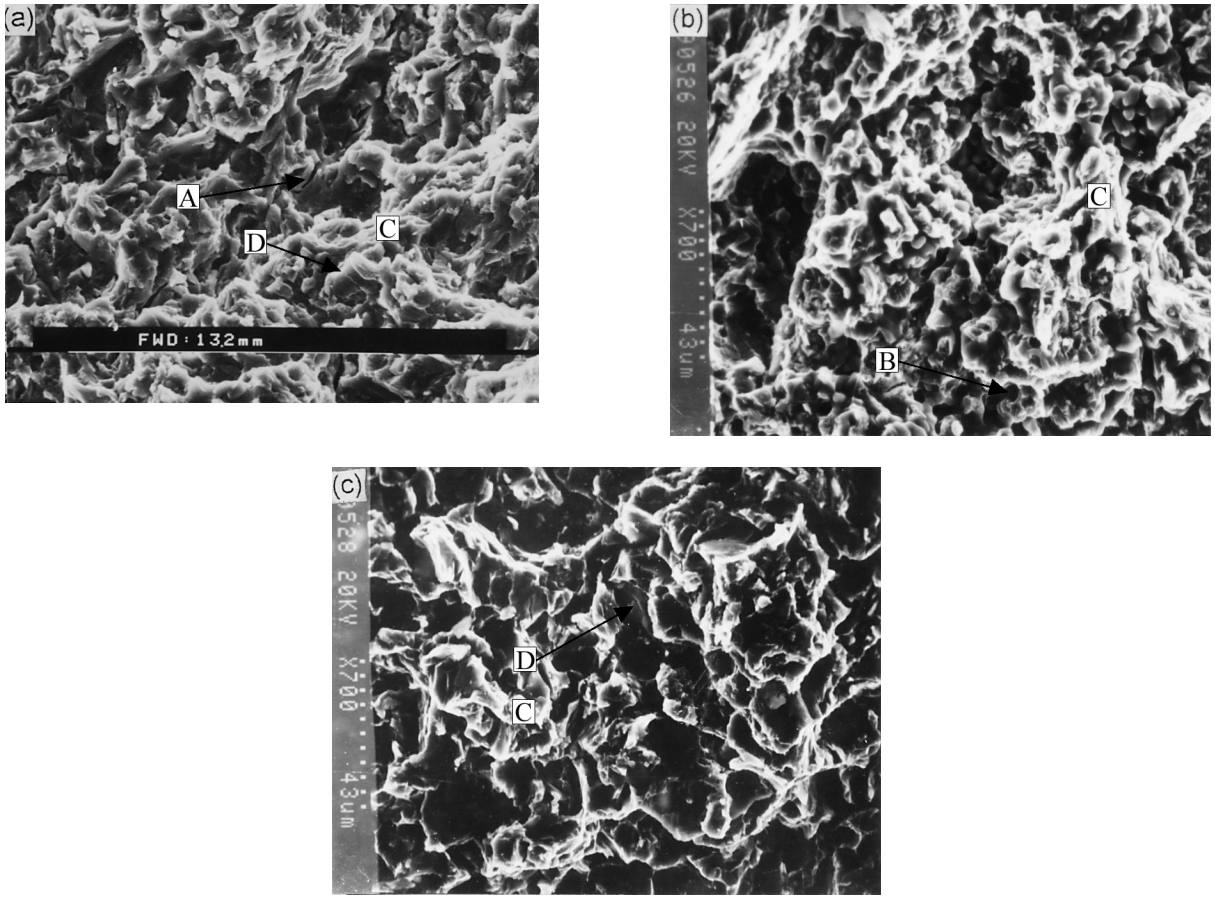

Fig. 14—Effects of Sb on the impact fractographs of AZ91 magnesium alloy: (*a*) AZ91, (*b*) AZ91 + 0.5Sb, and (*c*) AZ91 + 2Sb. A: secondary crack, B: quasi-cleavage dimple, C: deformation zone, and D: cleavage step.

shows that the grain is refined, and the amount of deformation tearing zone (at C in Figure 14) and quasi-cleavage dimples (at B in Figure 14(a) and (b)) increases with 0.5 wt pct Sb addition, which exhibits more obvious quasi-cleavage fracture features. At this time, impact toughness is increased. Figure 14(c) shows that the impact fractograph of AZ91 + 2.0Sb has smaller deformation zone (at C in Figure 14(c)), more cleavage steps (at D in Figure 14(c)), and again exhibits more obvious cleavage fracture features. As a result, the impact toughness is again reduced.

IV. CONCLUSIONS

1. With Sb addition into the AZ91 alloy, the grain is refined, $Mg_{17}Al_{12}$ phase is fined and granulated, and a new Mg_3Sb_2 phase is formed and becomes coarse needle-shaped as Sb content increases.
2. The room-temperature tensile strength, elongation, and impact toughness increase first, and then decrease with increasing Sb content, reaching their maximum when Sb content is 0.5 wt pct.
3. When composition is constant, the room-temperature tensile strength and elongation increase with the reduction of section thickness, when the section thickness is constant, the room-temperature tensile strength and elongation increase first, and then decrease with increasing Sb content, reaching their maximum when Sb content is 0.5 wt pct.
4. The addition of Sb into the AZ91 alloy increases the tensile strength of the studied Mg alloys at 100 °C and 150 °C. The tensile strength increases first, reaches a maximum when Sb content is 1 wt pct, and then decreases with increasing Sb content. The elongation increases first, reaches a maximum when Sb content is 1 wt pct, and then decreases with increasing Sb content at 100 °C; however, Sb addition reduces elongation at 150 °C.
5. The room-temperature tensile and impact fractographs of the studied magnesium alloys exhibit intergranular fracture features. The deformation zone enlarges first, and then reduces with increasing Sb content. Tensile fractographs are consistent with the change of tensile strength and elongation increasing first, and then decreasing with increasing Sb content. For impact fractographs, the quasi-cleavage fracture feature becomes obvious first, and then the cleavage fracture feature becomes obvious again with increasing Sb content, which is consistent with the change of impact toughness increasing first, and then decreasing with increasing Sb content.

ACKNOWLEDGMENTS

The authors express their thanks to the National Natural Science Foundation of China (Contract No. 59901007) and the Visiting Scholar Foundation of Key Lab at the University for financial support of this work.

REFERENCES

1. R.F. Brown: *Adv. Mater. Processes*, 1998, vol. 154 (3), pp. 31-33.
2. R.E. Brown: *International Magnesium Association, 54th Annual World Conf., Light Met. Age*, 1997, vol. 55 (7–8), pp. 72-75.
3. R.E. Brown: *International Magnesium Association, 55th Annual World Conf., Light Met. Age*, 1998, vol. 56 (7–8), pp. 86-93.
4. R.E. Brown: *Magnesium Alloys and Their Applications International Conf., Light Met. Age*, 1998, vol. 56 (7–8), pp. 94-98.
5. F.H. Froes, D. Eliezer, and E. Aghion: *JOM*, 1998, vol. 50 (9), pp. 30-34.
6. W.J. Park and N.J. Kim: *Scripta Metall. Mater.*, 1995, vol. 32 (11), pp. 1747-52.
7. A. Luo and M.O. Pekguleryuz: *J. Mater. Sci.*, 1994, vol. 29, pp. 5259-71.
8. C. Sanchez, G. Nussbaum, P. Azavant, and H. Octor: *Mater. Sci. Eng. A*, 1996, vol. 221 (1–2), pp. 48-57.
9. H. Baker: *Adv. Mater. Processes*, 1989, vol. 136 (3), pp. 35-36 and 39-42.
10. L. Duffy: *Mater. World*, 1996, vol. 4 (3), pp. 127-30.
11. M.O. Pekguleryuz and M.M. Avedesian: *J. Jpn Inst. Met.*, 1992, vol. 42 (12), pp. 679-86.
12. S. Khan and R. Elliott: *J. Mater. Sci.*, 1994, vol. 29 (3), pp. 736-41.
13. I.J. Polmear: *Recent Developments in Light Alloys, Mater. Trans., JIM*, 1996, vol. 37 (1), pp. 12-31.
14. Y. Carbonneau, A. Couture, and A.V. Neste: *Metall. Mater. Trans. A*, 1998, vol. 29A (6), pp. 759-63.
15. W.J. Park, H. Park, D.H. Kim, and N.J. Kim: *Mater. Sci. Eng. A*, 1994, vols. 179–180, pp. 637-40.
16. S. Lee, S.H. Lee, and D.H. Kim: *Metall. Mater. Trans. A*, 1998, vol. 29A (2), pp. 1221-35.
17. E.L. Lavernia, E. Gomez, and N.J. Grant: *Mater. Sci. Eng.*, 1987, vol. 95, pp. 225-36.
18. Yizhen Lu, Qudong Wang, Xiaoqin Zeng, and Wenjiang Ding: *Mater. Sci. Eng. A*, 2000, vol. 278, pp. 66-76.
19. A.A. Nayeb-Hashemi and J.B. Clark: *Bull. Alloy Phase Diagrams*, 1984, vol. 5 (6), pp. 579-84.